SSS-FR-94-14418

NUMERICAL SIMULATION OF QUARRY BLAST SOURCES

K. L. McLaughlin
T. G. Barker
J. L. Stevens

Maxwell Laboratories, Inc.
S-CUBED Division
P.O. Box 1620
La Jolla, CA 92038-1620

January 1994

Final Report

Phillips Laboratory
Kirtland Air Force Base, NM 87117-5320

REPORT DOCUMENTATION PAGE

Form Approved
OMB No. 0704-0188

1. AGENCY USE ONLY *(Leave blank)*	2. REPORT DATE	3. REPORT TYPE AND DATES COVERED
	1 January 1994	Final Report 09/16/91-12/15/93

4. TITLE AND SUBTITLE
NUMERICAL SIMULATION OF QUARRY BLAST SOURCES

5. FUNDING NUMBERS
F29601-91-C-DB27

6. AUTHOR(S)
K. L. McLaughlin, T. G. Barker and J. L. Stevens

7. PERFORMING ORGANIZATION NAME(S) AND ADDRESS(ES)
Maxwell S-CUBED Division
P.O. Box 1620
La Jolla, CA 92038-1620

8. PERFORMING ORGANIZATION REPORT NUMBER
SSS-FR-94-14418

9. SPONSORING/MONITORING AGENCY NAME(S) AND ADDRESS(ES)
ARPA-NMRO
3701 N. Fairfax Dr. #717
Arlington, VA 22203-1714

Phillips Laboratory (PL/PKVA)
3651 Lowry Avenue, SE
Kirtland, AFB, NM 87117-5777

10. SPONSORING/MONITORING AGENCY REPORT NUMBER

11. SUPPLEMENTARY NOTES

12a. DISTRIBUTION/AVAILABILITY STATEMENT
Approved for Public Release; Distribution Unlimited

12b. DISTRIBUTION CODE

13. ABSTRACT *(Maximum 200 words)*

This final report summarizes the principal results of numerical investigations of the quarry blast as a seismic source. The goal was to derive simple but physically meaningful models that could be used to predict regional and teleseismic waveforms for large industrial blasts. The source models may then be used to develop seismic discrimination strategies for the identification of industrial blasts and other natural and man made seismic sources.

Physical models are presented for the exicitation of seismic waves from quarry blasts. The effects of spall, ripple firing, and the quarry bench on the excitation of seismic waves are each investigated. Theoretical derivations are presented for physical models which consist of forces applied to the free surface to model spall and modifications to the explosion moment tensor to model the effects of the non-planar free surface of the quarry bench. Numerical investigations using both 2D and 3D finite difference calculations are used to verify that the simplifying assumptions are valid for the bandwidths of interest. It is concluded that the spall source should be an important part of the typical quarry blast and

14. SUBJECT TERMS			15. NUMBER OF PAGES
Nuclear Discrimination	Quarry Blast	Spall	
Synthetic Seismograms	Nuclear Testing	Finite Differences	16. PRICE CODE

17. SECURITY CLASSIFICATION OF REPORT	18. SECURITY CLASSIFICATION OF THIS PAGE	19. SECURITY CLASSIFICATION OF ABSTRACT	20. LIMITATION OF ABSTRACT
UNCLASSIFIED	UNCLASSIFIED	UNCLASSIFIED	

CLASSIFIED BY:

DECLASSIFY ON:

13. Abstract *(Continued)*

and that horizontal movement of material away from the quarry face should provide a source of additional S waves. A simple numerical model for the effects of the non-planar quarry face is to replace the non-deviatoric explosion moment tensor with a deviatoric moment tensor. Therefore the explosion behind a quarry face will appear non-isotropic and radiate more S waves than the explosion at the same depth in a layered half-space.

The scenario of hiding a decoupled or partially decoupled underground nuclear explosion in the quarry blast is considered given the model that was developed for the quarry blast. It is concluded that if the large industrial chemical explosion is ripple fired, the amplitude of the seismic signal is only 10% of the amplitude of a blast in which all explosives are detonated simultaneously. Consequently, the explosion will dominate a simultaneous bomb and ripple-fired quarry blast if the (tamped) explosion yield exceeds 10% of the total quarry yield. Finally, synthetic regional Pg and Lg excited by the quarry blast model with models for an overburied explosion, a normally buried explosion with spall, and a shallow crustal earthquake. Based on these models there is theoretical justification to believe that frequency dependence of Pg/Lg ratios and Lg spectra may contain discrimination information.

Table of Contents

List of Illustrations

List of Illustrations (Continued)

Numerical Simulation of Quarry Blast Sources

Summary

This final report summarizes the principal results of numerical investigations of the quarry blast as a seismic source. The goal was to derive simple but physically meaningful models that could be used to predict regional and teleseismic waveforms for large industrial blasts. The source models may then be used to develop seismic discrimination strategies for the identification of industrial blasts and other natural and man made seismic sources.

Physical models are presented for the excitation of seismic waves from quarry blasts. The effects of spall, ripple firing, and the quarry bench on the excitation of seismic waves are each investigated. Theoretical derivations are presented for physical models which consist of forces applied to the free surface to model spall and modifications to the explosion moment tensor to model the effects of the non-planar free surface of the quarry bench. Numerical investigations using both 2D and 3D finite difference calculations are used to verify that the simplifying assumptions are valid for the bandwidths of interest. It is concluded that the spall source should be an important part of the typical quarry blast and that horizontal movement of material away from the quarry face should provide a source of additional S waves. A simple numerical model for the effects of the non-planar quarry face is to replace the non-deviatoric explosion moment tensor with a deviatoric moment tensor. Therefore the explosion behind a quarry face will appear non-isotropic and radiate more S waves than the explosion at the same depth in a layered half-space.

The scenario of hiding a decoupled or partially decoupled underground nuclear explosion in the quarry blast is considered given the model that was developed for the quarry blast. It is concluded that if the large industrial chemical explosion is ripple fired, the amplitude of the seismic signal is only 10% of the amplitude of a blast in which all explosives are detonated simultaneously. Consequently, the explosion will dominate a simultaneous bomb and ripple-fired quarry blast if the (tamped) explosion yield exceeds 10% of the total quarry yield. Finally, synthetic regional Pg and Lg excited by the quarry blast model are compared with models for an overburied explosion, a normally buried explosion with spall, and a shallow crustal earthquake. Based on these models there is theoretical justification to believe that frequency dependence of Pg/Lg ratios and Lg spectra may contain discrimination information.

1.0 A physical model

The typical large quarry blast is designed to fracture and move large quantities of rock in a safe and economical manner. To accomplish this, explosives are placed at scaled burdens, $Q/W^{1/3}$, between 0.5 and 1 m per cube-root Kg of explosives (between 50 and 100 $m/Kt^{1/3}$) and detonated in many separate holes. Detonations are timed so as to allow the rock from one row of charges to move out of the way before the next row of charges are detonated. In this way, fracture from spallation is maximized. The blasting literature (Langefors and Kihlstrom, 1963) confirms that the spall momentum from charges detonated in this range of scaled burden is consistent with the spall momentum predicted by non-linear finite difference simulations of nuclear explosives in the same range of scaled depth of burial, $4 * 10^{10}$ Nt-sec per Kt explosive

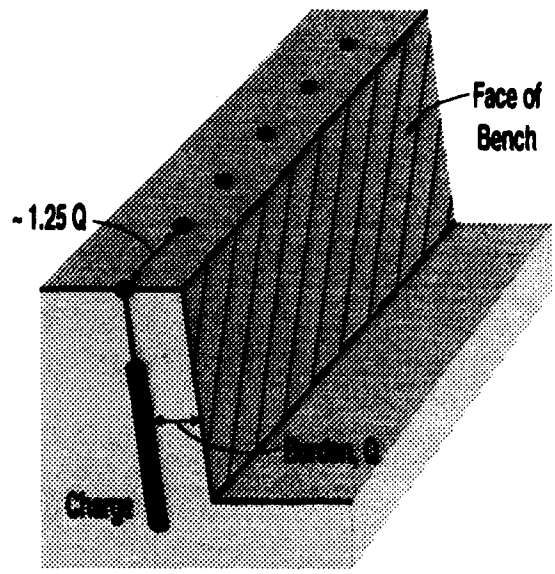

Figure 1.01 A typical quarry blast consists of multiple detonations of up to several tons each behind a quarry face.

or 40 Nt-sec per Kg of explosive. (see Barker, et al., 1993a).

See Appendix A for a more detailed derivation of the equivalent forces required to model the spall from a quarry face. We present here the principal conclusions of Barker et al. (1993a).

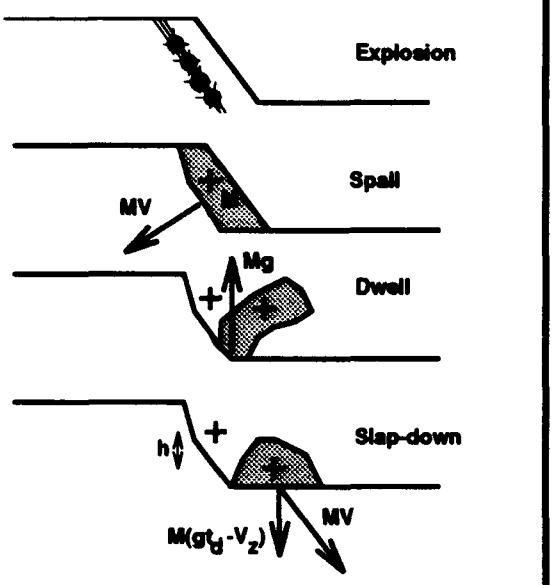

Figure 1.02 A physical model for the spall associated with a quarry blast. The explosions spall material from the face that then falls to the quarry floor. The spalled mass, M, may fall a net distance, h.

To describe the spall source for a quarry blast, we have adapted the spall model of Barker and Day (1990) to include the effects of horizontal throw and the net change in elevation of the spalled mass. Both of these effects are found to make significant contributions to the seismic source.

The equivalent vertical spall force is given by

$$F_z = M[V_{z0}\delta(t) + (gt_d - V_{z0})\delta(t-t_d) - g(H(t)-H(t-t_d))] \quad \text{(EQ 1)}$$

and the horizontal force is given by

$$F_x = M\,V_{x0}[\delta(t) - \delta(t - t_d)], \quad \text{(EQ 2)}$$

where M is the spall mass, V_{z0} and V_{x0} are the initial vertical and horizontal spall velocities, g is the acceleration of gravity, and t_d is the spall dwell time,

$$t_d = [V_{z0} + (V_{x0}^2 + 2h\,g)^{1/2}] / g, \quad \text{(EQ 3)}$$

and h is the net change in elevation of the spall mass. The total spall momentum is $P = M\,(V_{z0}^2 + V_{x0}^2)^{1/2}$. These forces are applied to the free surface. Note that if the initial horizontal velocity is zero and the net vertical elevation is zero, h=0, this model reverts to that described for vertical spall in Barker and Day (1990). The model both conserves momentum and accounts for energy derived from the net loss of potential gravitational energy. The only variables are the initial momentum, the total mass, and the direction of initial takeoff.

The time functions for these two force components are plotted in Figure 1.03. Obviously, the takeoff and slap-down phases are not as simple as delta functions, but the model contains the essential elements. The time functions in equations 1 and 2 can be made more detailed to reflect more complete knowledge of the spall ballistics.

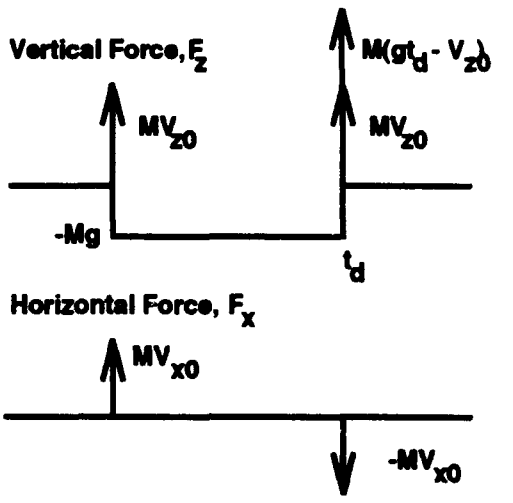

Figure 1.03 The dwell time is determined from the magnitude and direction of the takeoff velocity. If the spall mass falls a net distance, h, then there is a contribution from the gravitational potential.

We have computed Green's functions for point forces and moment tensor sources and convolved them with the spall and explosion source functions expected from a 20 ton explosion buried at a depth of 25 m. The results are shown in Figures 1.04 and 1.05. The spall is a significant source compared to the explosion.

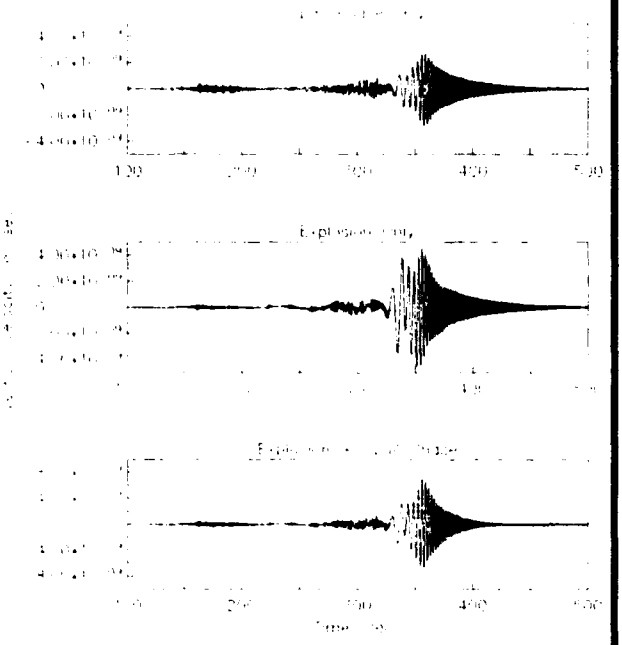

Figure 1.04 Comparison of the spall and explosion components of broadband seismograms

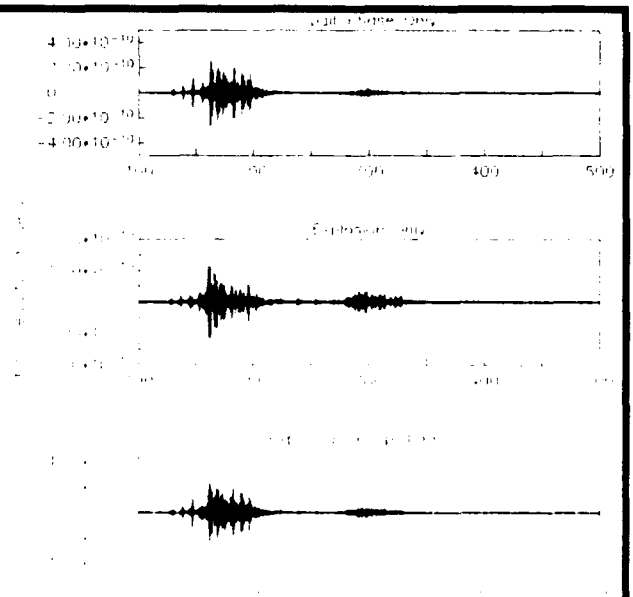

Figure 1.05 Comparison of the spall and explosion components of narrowband 0.75-5 Hz seismograms.

2.0 The hide in quarry blast scenario

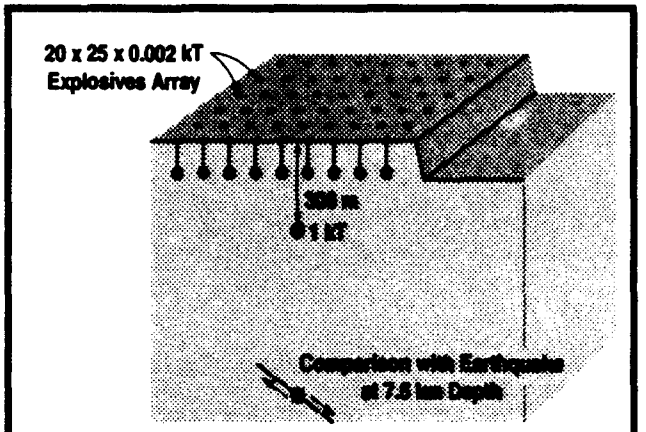

Figure 2.01 The hide in quarry blast scenario.

In the hide in quarry blast scenario, a large chemical shot designed to look like a quarry blast may be used to hide an overburied nuclear explosion. The nuclear explosion may be partially or fully decoupled. We have examined this scenario under the assumption that the shots are fired row-by-row as well as simultaneously. In order to detonate 1 Kt of chemical explosive using standard practices one scenario would be 500 charges of 2 metric tons each fired in rows of 25 each. Regional synthetic seismograms were produced at a distance of 1000 km for a quarry blast of 20 by 25 2-ton charges and for an overburied nuclear explosion of 1 Kt at a depth of 300m. This scenario is one of many such possible configurations, but it serves to illustrate our primary conclusions and is consistent with actual blasting practice.

The quarry blast synthetics were computed using the explosion plus spall model described in the previous section. Synthetics were examined for several cases, including pure vertical spall and spall with an initial angle of 45 degrees to the horizontal. Green's functions were computed from 0 to 5 Hz using a reflectivity code and convolved with the appropriate source time functions. The spall component of the quarry blast was found to be an important contribution to the quarry blast synthetic. Example synthetics are shown in Figure 2.02 (see also Figure 2.03) for

Figure 2.02 Vertical component synthetic seismograms (0.75-5 Hz) at 1000 km for the 1 Kt overburied bomb and the 1 Kt ripple fired quarry blast. The sum of the two is shown at the top. Note that the bomb dominates the ripple fired quarry blast. Note the different Pg/Lg ratio of the bomb and quarry blast. Note that the ripple fired quarry blast is not 500 times larger than the single 2 ton quarry blast shown at the bottom. This is because of the extended duration of the ripple fired quarry blast.

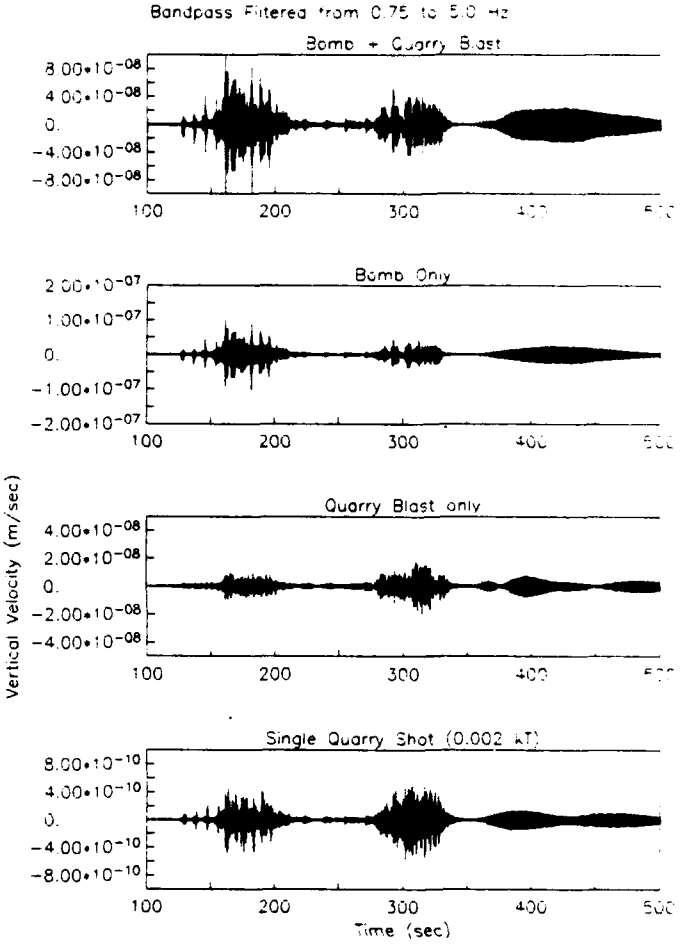

Figure 2.03 Predicted smoothed Pg spectra (top) at a distance of 1000 km for the1 Kt bomb (dashed line) and 1 Kt ripple fired quarry blast (solid line). A spectral ratio is shown below to illustrate the enhanced high frequencies in the overburied bomb.

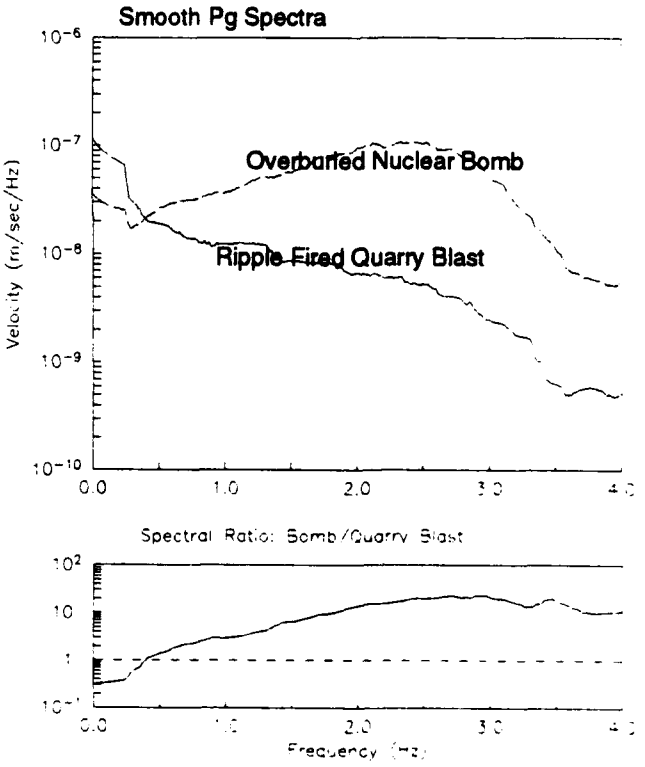

Figure 2.0.4 From top to bottom: synthetic seismograms (0.75-5 Hz) for the 1 Kt overburied explosion (Bomb) plus the 1 Kt simultaneous quarry blast, the 1 Kt overburied explosion only, the 1 Kt simultaneous quarry blast only, and a single 20 ton shot. Note that simultaneous detonation of 500 2-ton shots could obscure the the 1 Kt overburied explosion. For simultaneous detonation, the 1 Kt quarry blast is almost exactly 500 times larger than the single 20 ton shot.

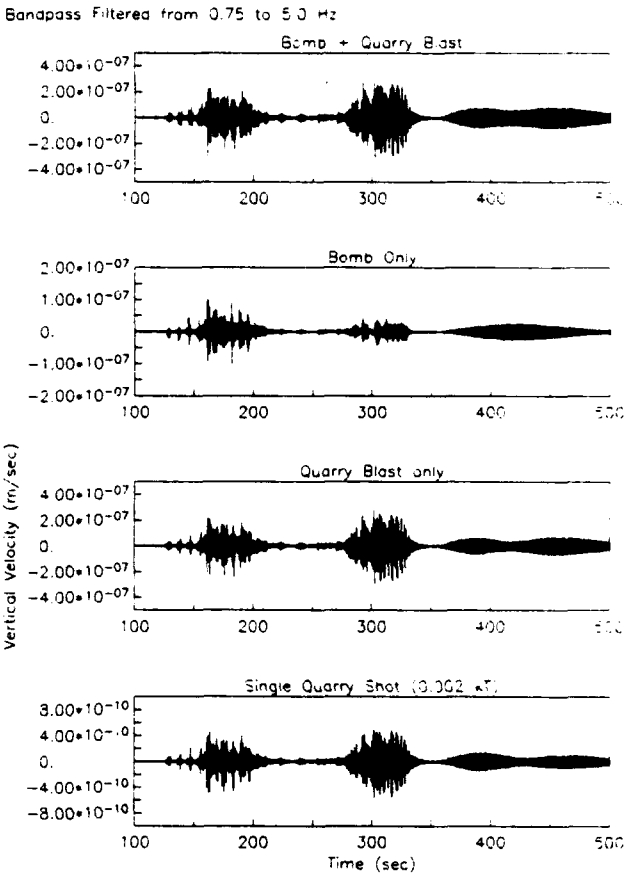

Figure 2.0.5 From top to bottom: synthetic seismogram spectra (0-5 Hz) for the 1 Kt overburied explosion (Bomb) plus the 1 Kt simultaneous quarry blast, the 1 Kt overburied explosion only, the 1 Kt simultaneous quarry blast only, and a single 20 ton shot. Note that simultaneous detonation of 20x25 2-ton shots could obscure the the 1 Kt overburied explosion. For simultaneous detonation, the 1 Kt quarry blast is almost exactly 500 times larger

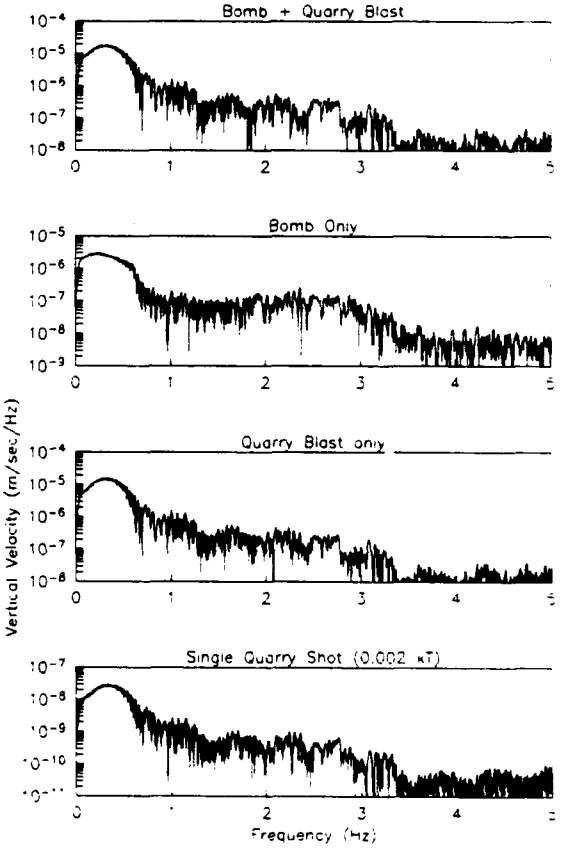

the 0.75-5 Hz bandwidth. Because the ripple fired quarry blast is detonated over an extended duration, the 500 2 ton blasts generate a signal an order of magnitude smaller than an amplitude 500 times the amplitude of each individual 2 ton blast. In order to hide the explosion, the 500 separate charges must be detonated nearly simultaneously. This is in general agreement with the results of Smith (1992).

We conclude that in order to hide an overburied nuclear explosion (bomb) with a seismic yield of 1 Kt, the 1 Kt of chemical explosives would have to be detonated nearly simultaneously. Even so, the overburied explosion may still be visible at high frequencies as anomalous high frequency energy in the quarry blast plus bomb seismogram (see Figures 2.04 and 2.05).

3.0 The effects of the quarry face

3.1 A theoretical model

A theoretical model for the effects of the quarry face has been proposed (Barker et al. 1993b). For a more detailed theoretical discussion, the reader is referred to Appendix B. The essence of this model is that for a moment tensor source located behind a non-horizontal surface such as a quarry face, the apparent horizontal couple perpendicular to the face is effectively reduced. Therefore an explosion source behind the quarry face no longer looks isotropic when compared to an explosion in a half-space. If we let the quarry face be aligned along the Y axis, then we can summarize this model by saying that the apparent moment tensor component, M_{xx}, is reduced from that of the actual moment tensor. The apparent moment tensor components for an explosion behind the face will obey the relation.

$$M_{xx} < M_{yy}, M_{yy} = M_{zz}. \quad \text{(EQ 4)}$$

The far-field seismic waveforms are then computed using the apparent moment tensor components and plane-layered Green's functions for a model without the quarry face.This model is valid for wavelengths long compared to the height of the bench.In order to illustrate this result, we have computed several numerical simulations using 2D and 3D linear finite difference codes.

3.2 2D finite difference modeling

2D linear finite difference calculations have been performed using reciprocity to examine the radiation efficiency of a point explosive source in the vicinity of a quarry face. A plane P or Rayleigh wave is incident upon a finite difference grid (Figure 3.2.1). The dilatation is then monitored on the finite difference grid. The dilatation for a model with free-surface topography (like a quarry) is then compared to dilatation in a half-space. Likewise displacements monitored in the grid are used to infer the radiation from point sources. The result is a map of the efficiency of radiation by sources in the finite difference model relative to sources in a half-space. The results are contoured in Figure 3.2.2 for a plane P-wave arriving from the right.

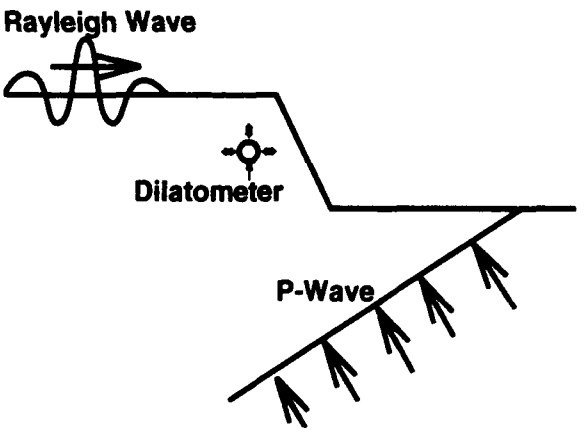

Figure 3.2.1 Reciprocity is used to infer the far-field radiation of P and Rayleigh waves by measuring dilatation and displacement at locations in the 2D grid from incident plane P and Rayleigh waves.

The results shown in Figure 3.2.2 have been found to be insensitive to the take-off angle of the P-wave. Similar results are found for Rayleigh waves arriving from either the right or the

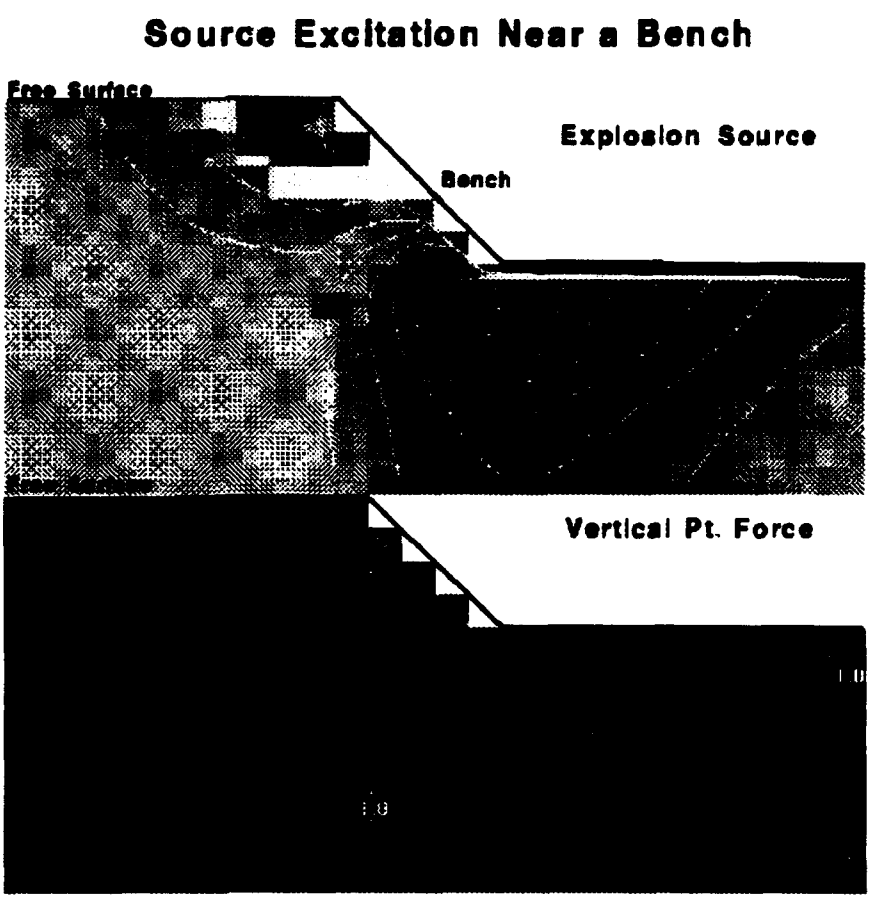

Figure 3.2.2 Excitation efficiency of a point source as a function of location behind a 45 degree quarry face. The moment tensor explosion source (top) is reduced by as much as 50% for locations behind the bench. At distances behind the bench greater than the bench height, the explosion source relative to the half-space is only reduced by 20% or less. At a location just below the toe of the quarry face, the explosion source is enhanced by a factor of 2 or more. The vertical point force source (bottom) is hardly affected by the presence of the quarry face.This analysis is valid for wavelengths much longer than the bench height.

left. In all cases, the excitation from a point explosive source at a distance behind the bench less than 1/2 the height of the bench is reduced by nearly 50% relative to excitation in a half-space.

Simulations using incident SV waves show that SV radiation is enhanced by the presence of the bench for the explosive sources relative to sources in a half-space. The explosion behind the bench appears more deviatoric.

The 2D simulations lead to several predictions. First, an explosion behind a quarry face will show reduced excitation of P-waves and Rayleigh waves in directions perpendicular to the quarry face compared to an explosion in a half-space. Point forces applied to the quarry face and behind the quarry face will not be so affected. Half-space Green's functions may be used to model the explosion but the explosion source should be replaced with a non-isotropic source with M_{xx} about 50% of $M_{yy} = M_{zz}$.

A corollary to the model that M_{xx} does not equal M_{yy} is that the explosion behind the quarry face will excite SH waves in a direction 45° to the bench face normal and there will be an azimuthally dependent radiation pattern to the P and SV waves. Although 2D modeling can not explore this conclusion directly, we can use 3D finite difference modeling to explore the azimuthal scattering of seismic waves generated by an explosion behind the bench.

3.3 3D finite difference modeling

A 3D finite difference calculation was performed that models a large quarry with vertical faces. A point explosive source was located directly behind the quarry face. The geometry of the quarry and explosion are shown in Figure 3.3.1. The Recursive Grid Refinement (RGR) version of TRES-3D was used to perform the calculation. A calculation without the quarry was computed for comparison.

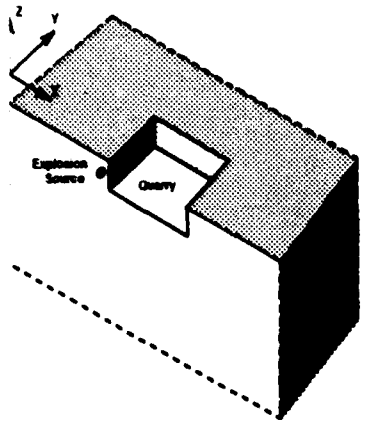

Figure 3.3.1 Geometry of the 3D finite difference calculation.

Some snap-shots of the particle velocity wavefield are shown in Figures 3.3.2 and 3.3.3. These snap-shots illustrate that the P-wave amplitudes are reduced for azimuths perpendicular to the quarry face. These results are consistent with the results of the 2D simulations. We observe non-isotropic radiation from the explosion source behind the quarry.

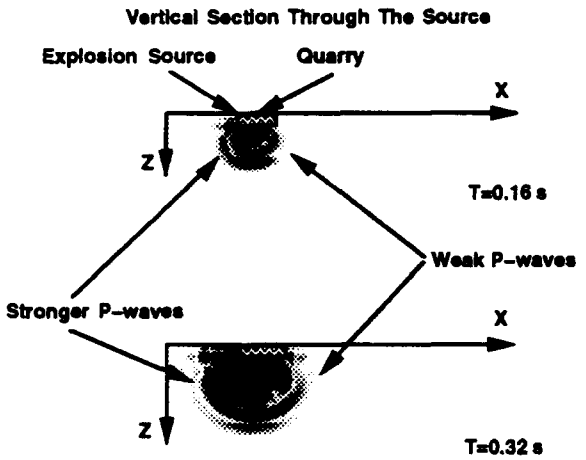

Figure 3.3.2 Vertical section from 3D finite difference simulation. The P-wave wavefront is clearly visible.

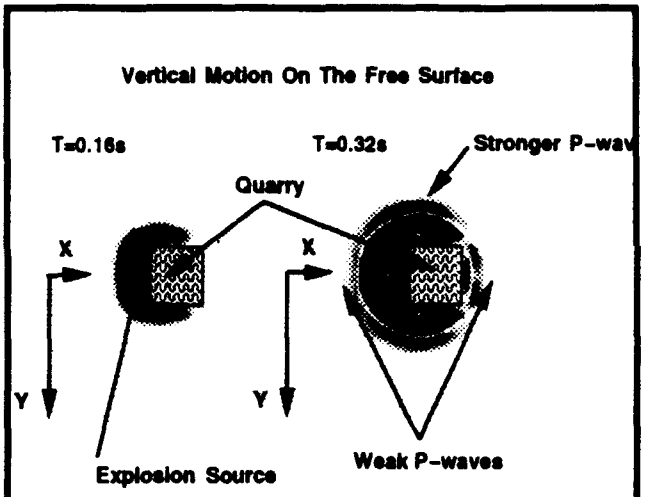

Figure 3.3.3 Vertical motion on the free surface of a 3D finite difference simulation showing the P-wave radiation from a point source behind the quarry face.

The 3D finite difference simulations show that the radiated P-wave is weakest in directions perpendicular to the quarry face, as if the M_{xx} component of the explosive source were reduced compared to the M_{yy} component. P-waves radiated parallel to the quarry face are not significantly different from the half-space case (no quarry). The explosion source behind the quarry face also radiates SH waves.

4.0 Discrimination

An important problem in discrimination is the identification of quarry blasts, earthquakes, normally buried nuclear explosions, and overburied or decoupled nuclear explosions. This problem is complicated by the fact that future events of interest will occur in areas where we have little or no prior experience in discriminating explosions and earthquakes. In particular, we expect that overburied and decoupled explosions will not have the characteristic spall signature of normally buried explosions. Even where we have experience with underground nuclear explosions and earthquakes, we have somewhat limited experience with overburied explosions. Most of our discrimination experience is based on normally buried explosions compared to earthquakes or on large quarry blasts compared to earthquakes. Therefore, numerical models of seismic sources may suggest useful discriminants for new areas of interest provided they can

be calibrated to regions for which we have more extensive discrimination experience.

In Figure 4.01 we show comparisons of predicted Pg/Lg spectral ratios for four different M_L=4 seismic sources at 1000 km: a thrust earthquake (depth 7.5 km), a ripple fired quarry blast, a normally buried explosion with spall, and an overburied explosion with no spall. The Lg/Pg ratio is scaled so that the ratio of the earthquake at 1 Hz is 10 and the Lg amplitude at 1 Hz is held nearly constant (M_L=4). The details of this figure depend on the crustal structures and particularly on the crustal Q's. However the qualitative prediction is that at frequencies above 2 Hz, we expect that the earthquake will have enhanced Lg/Pg ratios relative to those at 1 Hz, the normally buried bomb with spall will have the lowest Lg/Pg ratios at 3 Hz relative to those at 1 Hz, and the quarry blast and overburied or decoupled bomb will be intermediate. These predictions are consistent with observations of Bennett, et al. (1989). In studies of spectral slopes, they found

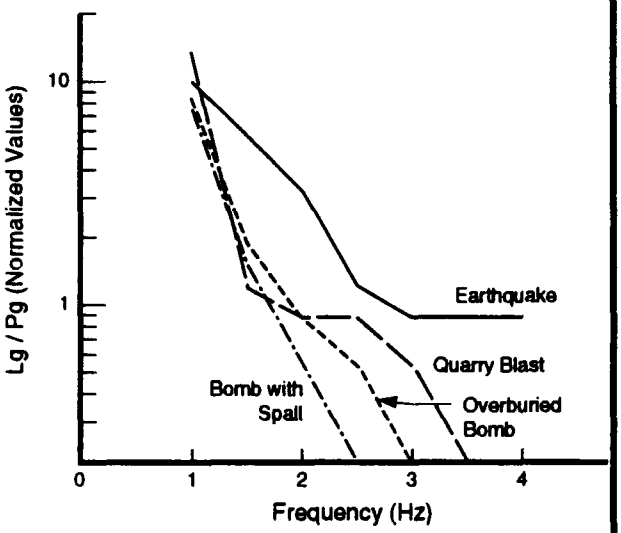

Figure 4.01 Lg/Pg spectral ratio at 1000 km for four sources. Spectra determined from smoothed envelopes of bandpass filtered seismograms.

that the ratio of Lg-to-P fell off faster with increasing frequency for normally buried bombs than earthquakes or quarry blasts. In Figure 4.02 we show predicted Lg spectra for the same four sources. The spectra are all normalized to 1 at 1 Hz. The quarry blast falls off faster than the earthquake spectrum also consistent with observations of Bennett et. al. (1989). Again the details of this plot will depend on the particular crustal model chosen, but we expect that some of the qualitative results will apply to a wide range of structures. Because of the spall components of the quarry blast and the normally buried bomb we expect that they will show the greatest spectral decay with increasing frequency. These results are in general agreement with results of Kim, et al. (1993), Wuster (1993), and Hutchenson and Herrmann (1993), for quarry blasts and earthquakes.

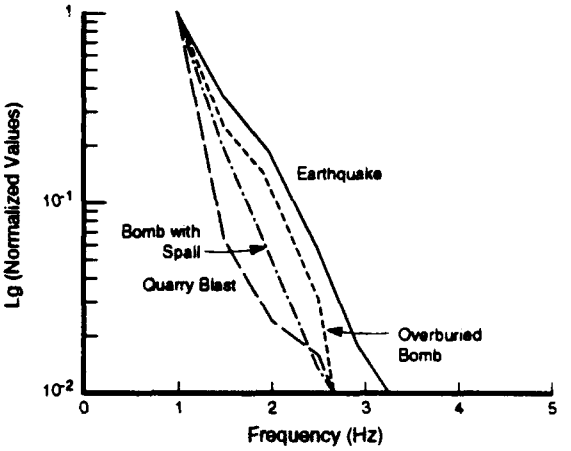

Figure 4.02 Normalized Lg spectra for four sources at 1000km. The earthquake is the most enriched in high frequency Lg.

5.0 Conclusions

We have proposed models for the "spall" contribution of the quarry blast and the effects of the quarry face on the explosive source. Detailed theoretical discussions are contained in Appendices A and B. These models may have significant implications on our ability to identify and discriminate large quarry blasts from earthquakes, rock-bursts, and nuclear explosions. These models for radiation from the spall source and explosion source behind the non-horizontal free-surface could be tested in a properly designed experimental program. We summarize our specific conclusions below.

- Seismic radiation from the spall part of a typical quarry blast is comparable to the explosion part of the quarry blast source.

- The quarry blast source is a band-limited signal compared to the overburied bomb due to the spall signal and the duration of the distributed quarry blast.
- Pg spectral values rise in the 0.5-3 Hz band for the overburied bomb but decay for the quarry blast source due to the spall contributions and duration of the quarry blast.
- Quarry blast spectra are scalloped primarily because of the duration of the source.
- The explosion will dominate a simultaneous bomb and ripple fired quarry blast if the (tamped) explosion yield exceeds 10% of the total quarry yield.
- Near simultaneous detonation of the entire quarry blast is required to hide an overburied nuclear explosion of comparable yield.
- Seismic amplitudes are insensitive to the direction of the spall as long as there is minimal elevation change.
- A net elevation change comparable to the burden can significantly increase the seismic amplitudes from a quarry blast.
- 2D simulations predict that P and Rayleigh radiation from a point explosion behind the quarry face may be reduced by a factor of50% due to the free-surface face.
- 2D simulations predict that the reduction in seismic signals radiated by a point explosion behind the quarry face for P-waves radiated perpendicular to the face is nearly independent of slowness.
- 2D simulations predict that seismic signals from the point force equivalents of spall are little affected by the free-surface face.
- 3D simulations predict that the free surface face introduces an azimuthal radiation pattern and generates SH waves.
- Source models for earthquake, quarry blast with spall, overburied explosion, and normally buried explosion with spall predict that frequency dependent Lg and Lg/Pg may serve as useful discriminants.

The proposed spall model for seismic radiation from quarry blasts predicts enhanced SV radiation compared to the point explosion source alone. Furthermore, the directivity of spall from a non-horizontal face predicts that SH waves will be generated. Both of these effects make quarry blasts look like deviatoric sources.

Because the dwell times for typical quarry blasts are near 1 sec, the typical quarry blast will have a peaked spectra and it is possible that this may lead to useful regional discriminants.

The recent results by Kim, *et al.* (1993), Hutchenson and Herrmann (1993), and Wuster (1993) are in qualitative agreement with our source models; small earthquakes are enriched in high frequencies relative to quarry blasts.

6.0 References

Aki, K. and P. G. Richards (1980). Quantitative Seismology Theory and Methods Volume 1, W. H. Freeman and Co., San Francisco, pp 557.

Barker, T. G. and S. M. Day (1990). A Simple Physical Model for Spall from Nuclear Explosions Based Upon Two-Dimensional Nonlinear Numerical Simulations, SSS-TR-90-11550

Barker, T. G., K. L. McLaughlin, J. L. Stevens (1993a). Numerical Simulation of Quarry Blast Sources, SSS-TR-93-13859.

Barker, T. G., K. L. McLaughlin, J. L. Stevens, and S. M. Day (1993b). Numerical Models of Quarry Blast Sources: the Effects of the Bench, SSS-TR-93-13915.

Bennett, T. J., B. W. Barker, K. L. McLaughlin, and J. R. Murphy (1989). Regional Discrimination of Quarry Blasts, Earthquakes, and Underground Nuclear Explosions, GL-TR-89-0114.

Hutchenson, K. D. and R. B. Herrmann (1993). Spectral Examination of the 16 June 1992 Earthquake and Quarry Blast Near Evansville, Indiana, *Seism. Res. Lett.*, 64, 169-184.

Kim, W.-Y., D. W. Simpson, and P. G. Richards (1993). Discrimination of Earthquakes and Explosions in the Eastern United States Using Regional High-Frequency Data, *Geop. Res. Lett.* 20, pp. 1507-1510.

Langefors, U., and B. Kihlstrom (1963). The Modern Techniques of Rock Blasting, John Wiley and Sons.

Smith, A. T. (1992). Discrimination of Explosions and Simultaneous Mining Blasts, LLNL Report UCRL-JC-109245.

Wuster, J. (1993). Discrimination of Chemical Explosions and Earthquakes in Central Europe - A Case Study, *Bull. Seism. Soc. Am.*, *83*, pp. 1184-1212.

Appendix A

Force Equivalents for Spall

Consider the situation that a volume of rock, V, in a face is moved along a surface, Σ (see Figure A-1 below). We can write the displacement, $U_i(\vec{X})$ at a far-field location, $\vec{X}$, using the representation theorem (Aki and Richards, 1980),

$$U_i(\vec{X}) = \int_{\Sigma} d\Sigma \upsilon_j(\vec{\eta})\, \delta u_k(\vec{\eta})\, C_{jkpq}(\vec{\eta})\, G_{ip,q}(\vec{X}, \vec{\eta})$$

where $U_i(\vec{X})$ is the i'th component of the far-field displacement at location $\vec{X}$, $\upsilon_j(\vec{\eta})$ is the normal at location, $\vec{\eta}$, on the surface Σ, $\delta u_j(\vec{\eta})$ is the displacement discontinuity across the surface Σ, $C_{jkpq}(\vec{\eta})$ is the elastic tensor, and $G_{ip,q}(\vec{X}, \vec{\eta})$ is the q'th derivative of the i'th component of the Green's tensor for displacement at $\vec{X}$ given a force in the p'th direction at location $\vec{\eta}$.

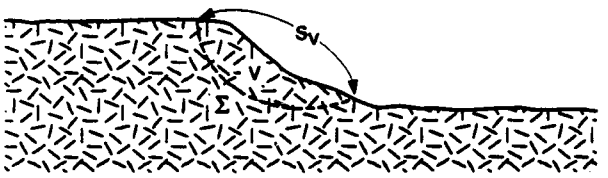

V – Spall Volume
Σ – Spall Surface
S_V – Free Surface of Spall Volume

Note that from reciprocity we can interpret,

$$T_{ik}(\vec{\eta}, \vec{X}) = \upsilon_j(\vec{\eta})\, C_{jkpq}(\vec{\eta}).G_{ip,q}(\vec{X}, \vec{\eta})$$

as the traction in the k'th direction at $\vec{\eta}$ due to a displacement in the i'th direction at $\vec{X}$.

We assume that $\delta u_j(\vec{\eta})$ is uncorrelated with $C_{jkpq}(\vec{\eta})\, G_{ip,q}(\vec{X}, \vec{\eta})$ on the surface, Σ. We discuss this assumption further below. We can rewrite our first equation as

$$U_i(\vec{X}) = \overline{\delta u_k} \int d\Sigma \upsilon_j(\vec{\eta})\, C_{jkpq}(\vec{\eta})\, G_{ip,q}(\vec{X}, \vec{\eta})$$

where

$$\overline{\delta u_k} = \frac{1}{A_\Sigma} \int_{\Sigma} d\Sigma \delta u_k(\vec{\eta})$$

and

$$A_\Sigma = \int_{\Sigma} d\Sigma$$

is the surface area. $\overline{\delta u_k}$ is the average displacement discontinuity across the surface, Σ. Since G_{ip} satisfies the equation of motion in V, we can write,

$$(C_{jkpq} G_{ip,q})_{,j} = -\rho\omega^2 G_{ik}$$

where ρ is the material density and $\omega = 2\pi f$ is the angular frequency. If we now integrate over the volume V and convert to a surface integral,

$$\int_V dV (C_{ikpq} G_{ip,q})_{,j} = \int_{(\Sigma + S_V)} d\Sigma \upsilon_j C_{jkpq} G_{ip,q}$$

where $(\Sigma + S_V)$ is the combined surfaces enclosing the volume V. S_V is a free surface, so the integral over it is zero and we have

$$\int_{\Sigma} d\Sigma \upsilon_j C_{jkpq} G_{ip,q} = -\omega^2 \int_V dV \rho G_{ik}$$

Now we denote by $\overline{G_{ik}}$, the average Green's tensor,

$$\overline{G_{ik}} = \frac{1}{M_V} \int_V dV \rho G_{ik}$$

and

$$M_V = \int_V dV \rho$$

is the total mass in the volume, V. And we can finally write,

$$u_i(\vec{X}) = -\omega^2 \overline{\delta u_k} M_V \overline{G_{ik}}$$

where the seismic source is a force proportional to the average acceleration time history of the spall mass. Note that the acceleration is averaged over the surface of the spall mass while the Green's function is averaged over the volume of

the spall mass. To further interpret these results, we define,

$$P_k = i\omega\overline{\delta u_k} M_V$$

as the k'th component of the equivalent spall momentum. Then the equivalent force is simply the time derivative of the spall momentum,

$$u_i(\vec{X}) = -i\omega P_k \overline{G_{ik}} = F_k \overline{G_{ik}}$$

It is easy to interpret this result. As the material moves away from the face, there is a recoil force. The spall temporarily carries away with it the momentum of the material at the face. The material then falls and/or slides down the face. These resulting impact and frictional forces bring the material to a halt. The recoil and impact forces are in opposite directions. Unlike the explosion spall from a contained nuclear explosion, the forces are not purely vertical. If we assume the material spalling away from the quarry face behaves as a ballistic, then we can write the equivelent forces as equations 1 through 3.

We now briefly discuss the conditions that permit the factoring of the equation to arrive at our result. This assumption that δu_k is uncorrelated with $C_{jkpq}G_{ip,q}$ on the surface is equivalent to the equation,

$$\int_\Sigma d\Sigma \, (\delta u_k - \overline{\delta u_k}) \, (\upsilon_j C_{jkpq} G_{ip,q} - \overline{\upsilon_j C_{jkpq} G_{ip,q}}) = 0$$

where the overbar indicates the average over the surface. Note that from the reciprocity theorem, we can interpret

$$T_{ik}(\vec{\eta}, \vec{X}) = \upsilon_j(\vec{\eta}) \, C_{jkpq}(\vec{\eta}) \frac{\partial G_{ip}}{\partial \eta_q}(\vec{X}, \vec{\eta})$$

as the traction in the k'th direction at $\vec{\eta}$ due to a displacement in the i'th direction at $\vec{X}$. One interpretation is that the displacement discontinuity on the surface, δu_k, is well represented by its average, $\overline{\delta u_k}$. This is a reasonable assumption since the variations in the displacement discontinuity will excite only high frequencies waves and cancel out in the far-field. A second interpretation is that this equation says that the tractions on the surface from a far-field source, $T_{ik}(\vec{\eta}, \vec{X})$, are well represented by their average over the surface, $\overline{T_{ik}(\vec{\eta}, \vec{X})}$. Again this is a resonable approximation for wavelengths longer than the size of the quarry face that has spalled. If these conditions are met, then we can write ,

$$\int_\Sigma d\Sigma \delta u_k \upsilon_j C_{jkpq} G_{ip,q} = \overline{\delta u_k} \int_\Sigma d\Sigma C_{jkpa} G_{ip,q}$$

which leads to our main result.

Appendix B

Effects of the Quarry Face

We are interested in the effective radiation pattern from an explosion source behind a quarry bench. The geometry is shown below. The point explosion source is located at $\eta_1 = 0$, a distance, h, to the left of the vertical bench. h is referred to as the burden of the quarry blast. Typical quarry blast practice is to choose a burden between 30 percent and 100 percent the height of the bench.

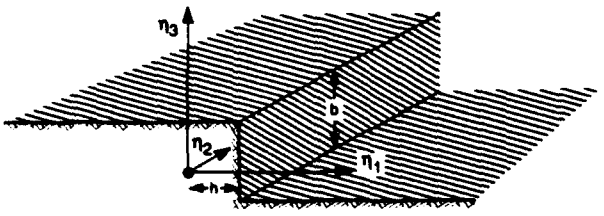

b = Bench Height
h = Burden or Source Distance to Bench Face

The seismic displacement at a location, $\vec{X}$, from an explosion source with moment tensor, $M_{ij} = \delta_{ij} M_o$ at location $\vec{\eta}$ may be written as

$$U_i(\vec{X}) = \frac{M_o}{3K(\vec{\eta})} C_{kkpq}(\vec{\eta}) G_{ip,q}(\vec{X}, \vec{\eta})$$

where $U_i(\vec{X})$ is the i'th component of displacement at location, $\vec{X}$, $K = \lambda + 2\mu/3$ is the bulk modulus at the source location, $C_{ijpq}(\vec{\eta})$ is the elastic tensor, and $G_{ip,q}(\vec{X}, \vec{\eta})$ is the q'th derivative of the Green's tensor response for the i'th component of motion at $\vec{X}$ given a force in the p'th direction at location $\vec{\eta}$.

Note that by reciprocity,

$$C_{kkpq}(\vec{\eta}) G_{ip,q}(\vec{X}, \vec{\eta}) = \sigma_{11}(\vec{\eta}) + \sigma_{22}(\vec{\eta}) + \sigma_{33}(\vec{\eta})$$

where σ_{11}, σ_{22} and σ_{33} are stress terms at location $\vec{\eta}$ due to a displacement in the i'th direction at location $\vec{X}$. We now make use of this reciprocal problem, where σ_{ij} is the stress tensor at $\vec{\eta}$ due to a displacement at $\vec{X}$. Similarly, we will write u_j as the displacement at $\vec{\eta}$ due to a displacement at $\vec{X}$. Dependence on the location $\vec{X}$ and the i'th direction of motion is suppressed for clarity of notation in the following discussion.

Now, we know on the vertical bench (a vertical free surface) that $\sigma_{11} = 0$, and we expand the η_1 dependence of σ_{11} in a Taylor's expansion from the bench.

$$\sigma_{11}(\eta_1 = 0) = \sigma_{11}(\eta_1 = h) - h \frac{\partial \sigma_{11}}{\partial \eta_1}\Big|_{\eta_1 = h}$$

$$= -h \frac{\partial \sigma_{11}}{\partial \eta_1}\Big|_{\eta_1 = h}$$

We have the equation of motion which states that

$$\frac{\partial \sigma_{11}}{\partial \eta_1}\Big|_{\eta_1 = h} + \frac{\partial \sigma_{12}}{\partial \eta_2}\Big|_{\eta_1 = h} + \frac{\partial \sigma_{13}}{\partial \eta_3}\Big|_{\eta_1 = h} = \rho \ddot{u}_1(h)$$

together with the free surface boundary conditions on the bench (at $\eta_1 = h$)

$$\frac{\partial \sigma_{12}}{\partial \eta_2}\Big|_{\eta_1 = h} = \frac{\partial \sigma_{13}}{\partial \eta_3}\Big|_{\eta_1 = h} = 0$$

hence we can state for the horizontal equation of motion on the bench

$$\frac{\partial \sigma_{11}}{\partial \eta_1}\Big|_{\eta_1 = h} = \rho \ddot{u}_1(\eta_1 = h)$$

Therefore,

$$\sigma_{11}(\eta_1 = 0) = -h \rho \ddot{u}_1(\eta_1 = h)$$

We approximate $\ddot{u}_1(\eta_1 = h)$ by the halfspace solution, $\ddot{u}_1^{(HS)}(\eta_1 = h)$, and we can write .

$$\sigma_{11}(\eta_1 = 0) \approx -h\,\rho\,\ddot{u}_1^{(HS)}(\eta_1 = h)$$

This says that the σ_{11} stress from a displacement source at location $\bar{x}$ is proportional to the distance from the bench, h, and density, ρ.

How much is the explosion behind a bench reduced with respect to an explosion in a halfspace? We can estimate this effect by writing the expression for the halfspace σ_{11} component of stress in terms of the halfspace displacements,

$$\sigma_{11}^{(HS)} = (\lambda + 2\mu)\frac{\partial u_1^{(HS)}}{\partial \eta_1} + \lambda\left(\frac{\partial u_2^{(HS)}}{\partial \eta_2} + \frac{\partial u3^{(HS)}}{\partial \eta_3}\right)$$

To estimate the ratio $\Gamma = \frac{\sigma_{11}}{\sigma_{11}^{(HS)}}$ we neglect the second term to get .

$$\sigma_{11}^{(HS)} \approx \rho\,\alpha^2\,\frac{\partial u_1^{(HS)}}{\partial \eta_1}$$

We note that for plane P waves propagating in the η_1 direction we can make the approximation that

$$\left|\frac{\partial u_1^{(HS)}}{\partial \eta_1}\right| \approx \frac{\omega}{\alpha}\left|u_1^{(HS)}\right|$$

so we have that

$$\Gamma = \frac{\sigma_{11}}{\sigma_{11}^{(HS)}} \approx \frac{\rho h \omega^2 u_1^{(HS)}}{\rho \alpha \omega u_1^{(HS)}} = \frac{\omega h}{\alpha} = kh$$

For, h = 10 m, α = 2000 m/s, we have Γ(10Hz) = 0.31, Γ(5Hz) = 0.15, and Γ(1Hz) = 0.031. This would indicate that the P-waves radiated perpendicular to the bench will be substantially reduced with respect to the half-space for much of the bandwidth of regional seismograms.

However, it is clear that the radiation pattern from an explosion behind the quarry bench will depend upon the slowness and the azimuth of the radiated wave. That is to say that $\Gamma = \Gamma(\bar{k}, h)$. A complete treatment of this problem therefore requires the solution of the complete scattering problem using numerical techniques as in the section 3.

DISTRIBUTION LIST
NON-GOVERNMENT CONTRACTORS

Prof. Thomas Ahrens
Seismological Lab, 252-21
Div. of Geol. & Planetary Sciences
California Institute of Technology
Pasadena, CA 91125

Dr. T. Bache, Jr.
Dr. Thomas J. Sorena, Jr.
Science Appl. Int'l Corp.
10260 Campus Point Drive
San Diego, CA 92121

Dr. Peter Basham
Dr. Robert North
Earth Physics Branch
Geological Survey of Canada
1 Observatory Crescent
Ottawa, Ontario, Canada K1A 0Y3

Dr. Douglas R. Baumgardt
Dr. Zoltan Der
ENSCO, Inc.
5400 Port Royal Road
Springfield, VA 22151-2388

Prof. Jonathon Berger
IGPP, A-025
Scripps Inst. of Oceanography
University of California, San Diego
La Jolla, CA 92093

Dr. G. A. Bollinger
Department of Geological Sciences
Virginia Polytechnic Institute
21044 Derring Hall
Blacksburg, VA 24061

The Librarian
Dr. J. Carter
Dr. Stephen Bratt
Center for Seismic Studies
1300 N. 17th Street, Suite 1450
Arlington, VA 22209-3871

Michael Browne
Teledyne Geotech
3401 Shiloh Road
Garland, TX 75041

Dr. Lawrence J. Burdick
Woodward-Clyde Consultants
566 El Dorado Street
Pasadena, CA 91109-3245

Dr. Theodore Cherry
Science Horizons, Inc.
710 Encinitas Blvd., Suite 200
Encinitas, CA 92024

Dr. Kin Yip Chun
Geophysics Division
Physics Department
University of Toronto
Ontario, Canada M5S 1A7

Dr. Paul M. Davis
Dept. Earth & Space Sciences
University of California (UCLA)
Los Angeles, CA 90024

Prof. Steven M. Day
Department of Geological Sciences
San Diego State University
San Diego, CA 92182

Dr. Mark D. Fisk
Mission Research Corporation
735 State Street
P.O. Drawer 719
Santa Barbara, CA 93102

Prof. Stanley Flatte
Applied Sciences Building
University of California
Santa Cruz, CA 95064

Dr. Roger Fritzel
Pacific Sierra Research
1401 Wilson Blvd., Suite 1100
Arlington, VA 22209

Dr. Holly K. Given
Inst. Geophys. & Planet. Phys.
Scripps Inst. Oceanography (A-025)
University of California-San Diego
La Jolla, CA 92093

Prof. Hans-Peter Barjos
Institute for Geophysik
Ruhr University/Bochum
P.O. Box 102148
4630 Bochum 1, FRG

Prof. Donald V. Helmberger
Seismological Laboratory
Div. of Geol. & Planetary Sciences
California Institute of Technology
Pasadena, CA 91125

Prof. Eugene Herrin
Prof. Brian Stump
Inst. for Study of Earth and Man
Geophysical Laboratory
Southern Methodist University
Dallas, TX 75275

Prof. Bryan Isacks
Prof. Muawia Barazangi
Cornell University
Department of Geological Sciences
SNEE Hall
Ithaca, NY 14850

Prof. Lane R. Johnson
Prof. Thomas V. McEvilly
Seismographic Station
University of California
Berkeley, CA 94720

Dr. R. Kemerait
ENSCO, Inc.
445 Pineda Court
Melbourne, FL 32940

Prof. Brian L. N. Kennett
Research School of Earth Sciences
Institute of Advanced Studies
G.P.O. Box 4
Canberra 2601, Australia

Dr. Richard LaCoss
MIT-Lincoln Laboratory
M-200B
P.O. box 73
Lexington, ?MA 02173-0073

Prof. Fred K. Lamb
University of Illinois
Dept. of Physics
1110 West Green Street
Urbana, IL 61801

Prof Charles A. Langston
Geosciences Department
403 Deike Building
The Pennsylvania State University
University Park, PA 16802

Prof. Thorne Lay
Dr. Susan Schwartz
Institute of Tectonics
Earth Science Board
Univ. of California, Santa Cruz
Santa Cruz, CA 95064

Prof. Arthur Lerner-Lam
Prof. Paul Richards
Prof. C. B. Scholz
Lamont-Doherty Geol. Observatory
Columbia University
Palisades, NY 10964

Dr. Manfred Hanger
Fed. Inst. for Geosci. & Nat'l Res.
Postfach 510153
D-3000 Hanover 51, FRG

Dr. Peter Marshall
Procurement Executive
Ministry of Defense
Blacknest, Brimpton
Reading FG7-4RS, United Kingdom

Dr. Randolph Martin, III
New England Research, Inc.
76 Olcott Drive
White River Junction, VT 05001

Dr. Bernard Maseinon
Societe Radiomana
27 rue Claude Bernard
75005 Paris, France

Dr. Gary McCartor
Prof. Henry L. Gray
Department of Physics
Southern Methodist University
Dallas, TX 75275

Dr. Keith L. McLaughlin
S-CUBED, A Div. of Maxwell Laboratories, Inc.
P.O. Box 1620
La Jolla, CA 92038-1620

Dr. Pierre Mecheler
Societe Radiomana
27 rue Claude Bernard
75005 Paris, France

Prof. Bernard Minster
Prof. John Orcutt
IGPP, A-025
Scripps Inst. of Oceanography
University of California, San Diego
La Jolla, CA 92093

Prof. Brian J. Mitchell
Dr. Robert Herrmann
Dept. Earth & Atmos. Sci.
St. Louis University
St. Louis, MO 63156

Mr. J. Murphy
Maxwell Laboratories, Inc.
S-CUBED Reston Geophysics Office
11800 Sunrise Valley Dr., Suite 1212
Reston, VA 22091

Dr. Jay J. Pulli
Radix Systems, Inc.
2 Taft Court, Suite 203
Rockville, MD 20850

Dr. Frode Ringdal
Dr. Svain Mykkeltveit
NTNF/NORSAR
P.O. Box 51
N-2007 Kjeller, Norway

Dr. Wilmer Rivers
Teledyne Geotech
314 Montgomery Street
Alexandria, VA 22314

Dr. Richard Sailor
TASC, Inc.
55 Walkers Brook Drive
Reading, MA 01867

Prof. Charles G. Sammis
Prof. Kei Aki
Center for Earth Sciences
University of Southern California
University Park
Los Angeles, CA 90089-0741

Prof. David G. Simpson
Lamont-Doherty Geol. Observatory
Columbia University
Palisades, NY 10964

Dr. Stewart W. Smith
Geophysics AK-50
University of Washington
Seattle, WA 98195

Prof. Clifford Thurber
Prof. Robert P. Meyer
University of Wisconsin-Madison
Dept. of Geology & Geophysics
1215 West Dayton Street
Madison, WS 53706

Prof. M. Nafi Toksoz
Prof. Anton Dainty
Earth Resources Lab
Massachusetts Inst. of Technology
42 Carleton Street
Cambridge, MA 02142

Prof. Terry C. Wallace
Dept. of Geosciences
Building 77
University of Arizona
Tucson, AZ 85721

Dr. William Wortman
Mission Research Corporation
735 State Street
P.O. Drawer 719
Santa Barbara, CA 93102

U.S. GOVERNMENT AGENCIES

Mr. Alfred Lieberman
ACDA/VI-OA, Room 5726
320 21st Street, N.W.
Washington, D.C. 20451

Colonel Jerry J. Perrizo
AFOSR/NP, Building 410
Bolling AFB
Washington, DC 20031-6448

Dr. R. Blandford
AFTAC/CSS
1300 N. 17th Street, Suite 1450
Arlington, VA 22209-3871

AFTAC/CA
STINFO
Patrick AFB, FL 32925-6001

Dr. Frank F. Pilotte
HQ AFTAC/TT
Patrick AFB, FL 32925-6001

Katie Polay
CIA-ACIS/TMC
Room 4X16NHB
Washington, DC 20515

Dr. L. Turnbull
CIA-OSWR/NED
Washington, DC 20505

Dr. R. Alewine and Dr. A. Ryall
ARPA/NMRO
3701 N. Fairfax Drive, Suite 717
Arlington, VA 22203-1714

ARPA/OASB/Librarian
3701 Fairfax Dr., Suite 717
Arlington, VA 22203-1714

Dr. Dale Glover
DIA/DT-1B
Washington, DC 20301

Dr. Michael Shore
Defense Nuclear Agency/SPSS
6801 Telegraph Road
Alexandria, VA 22310

Mr. Max A. Koontz (DP-5)
Department of Energy
Forrestal Building
1000 Independence Avenue, S.W.
Washington, DC 20585

Defense Technical Information Center
Cameron Station
Alexandria, VA 22314

Dr. John J. Cipar, PL/LWH
Phillips Lab/Geophysics Directorate
Hanscom AFB, MA 01731

Mr. J. Lewkowicz, PL/LWH
Phillips Lab/Geophysics Directorate
Hanscom AFB, MA 01731

Phillips Lab (PL/XO)
Hanscom AFB, MA 01731

Dr. J. Hannon and Dr. K. Nakanishi
Lawrence Livermore Natn'l Laboratory
P.O. Box 808
Livermore, CA 94550

Office of the Secretary of Defense
DDR&E
Washington, DC 20330

Eric Chael
Division 9241
Sandia Laboratory
Albuquerque, NM 87175

Dr. William Leith
U.S. Geological Survey
Mail Stop 928
Reston, VA 22092

Dr. Robert Masse
Box 25046, Mail Stop 967
Denver Federal Center
Denver, CO 80225

Directed Energy Effects
PL/WSM
Kirtland, NM 87117-5776